Article

Electrochemical system analysis from impedance data to system identification

Michael A. Danzer, Christian Plank, Tom Rüther

danzer@uni-bayreuth.de

Highlights

Data-driven, automated analysis of impedance data from electrochemical systems

Systems-theoretical approach for process identification and model reduction

Minimal model order without overfitting based on Shannon entropy of residuals

Analysis of power sources including batteries, fuel cells, and double-layer capacitors

Electrochemical impedance spectroscopy is used for operando characterization of electrochemical systems, but state-of-the-art impedance analysis techniques rely on model fitting and expert knowledge. Here, Danzer et al. develop an automated electrochemical system analysis that yields minimal order models without overfitting, providing a reliable, reproducible, and user-independent analysis.

Article

Electrochemical system analysis from impedance data to system identification

Michael A. Danzer,[1,2,3,*] Christian Plank,[1,2] and Tom Rüther[1,2]

SUMMARY

Electrochemical impedance spectroscopy is a non-destructive experimental technique for the operando characterization of electrochemical systems. Here, we develop electrochemical system analysis (ELSA) as a data-driven, systems-theoretical approach to the analysis of measured impedance spectra. It solves the problem of finding an interpretable model description that explains given impedance data with high accuracy and without prior model assumptions. ELSA adopts the comprehensive analysis of the generalized distribution of relaxation time analysis and builds upon the data-driven and regularization-free Loewner method. ELSA systematically interprets the transfer function resulting from the Loewner method to reliably identify serial elements and resistive-capacitive and resistive-inductive processes with characteristic time constants. It also finds resonant elements by identifying conjugate complex poles. Based on the Shannon entropy of the residuals and the curvature of the locus, ELSA automatically and reproducibly identifies the minimal model order, thus avoiding overfitting. System characterization results are presented for different types of electrochemical power sources: batteries, fuel cells, and double-layer capacitors.

INTRODUCTION

From a systems theory perspective, technical systems can be categorized as finite-dimensional, mostly non-linear systems with real inputs and outputs and an unknown number of internal states. A fundamental requirement for system identification is time invariance, i.e., the device under test does not change its properties and behavior during the measurement time. In order to characterize and analyze technical systems experimentally, the system under investigation is subjected to an excitation (input), and the system response (output) is observed. In general, the goal of system identification can be formulated as a state-space realization problem: find a state-space description of minimal order that explains the given data[1] without overfitting and without systematic residuals. Typical and experimentally available data of the devices to be analyzed are impulse response, step response, and frequency response, such as impedance data.

The accessibility of system properties is limited to observable states[2] and structurally identifiable parameters.[3–5] This means that states and parameters that cannot be reached by the system excitation and do not affect the system response cannot be identified, characterized, and analyzed using this set of input and output signals. If states and parameters are not observable and structurally identifiable, then complementary input/output signals may be found. If not, then fewer states can be observed, only lumped elements can be identified, or the system properties cannot

[1]Chair of Electrical Energy Systems, University of Bayreuth, Bayreuth, Germany

[2]Bavarian Center for Battery Technology, University of Bayreuth, Bayreuth, Germany

[3]Lead contact

*Correspondence: danzer@uni-bayreuth.de

https://doi.org/10.1016/j.xcrp.2024.102091

be analyzed non-destructively. Note S3 provides a brief discussion of observability and structural identifiability of state-space descriptions.

The challenges of non-destructive and data-driven system identification are listed as requirements for the electrochemical system analysis (ELSA).

(1) preventing strong model assumptions such as types of processes and model descriptions and model order
(2) identifying characteristic parameters such that the system description matches the given data with high accuracy
(3) finding physically interpretable parameters, e.g., positive parameters for passive systems
(4) preventing overfitting and identifying the minimal order of the state-space description

Impedance spectroscopy is widely used as a non-destructive experimental technique for the operando characterization of systems. It provides valuable insights into various applications, including sensors and power sources. Electrochemical impedance spectroscopy (EIS) is based on a harmonic system excitation and the monitoring of the system response. When applied to multi-cell systems, it offers valuable information on cell-to-cell variations[6,7] and the analysis of inhomogeneities.[8] EIS results are relevant for design, performance evaluation,[9–11] process identification,[12–15] and aging analysis.[16–18] For electrochemical systems, such as batteries, fuel cells, and electrolyzers, EIS is a powerful and versatile method for experimental characterization at many different levels, covering materials, components, cells, and systems.[13] The measured spectra contain a multitude of information on diffusion, conductance, charge transfer, interfaces, and interphases, as well as double layers. Besides time invariance, the prerequisite for a valid EIS measurement is linearity at each measurement point. For non-linear systems, this is satisfied for each frequency point by small excitation amplitudes, i.e., linearization at an operating point. However, the ensemble of impedance values across the frequency range illustrates the non-linear behavior, such as Warburg diffusion. The standard approach for EIS analysis involves fitting impedance models to impedance data.[13,19,20] EIS operates on a sound scientific basis and provides model functions for numerous electrochemical and physicochemical processes and systems.[21] However, the use of textbook impedance analysis, which involves fitting physico-chemical models to measured impedance data, is discussed with caution due to its strong model assumptions, such as type and number of processes, model order, and the selection of initial parameter values.[20,22,23] In many cases, the identifiability of model parameters and the observability of internal states cannot be guaranteed.[3,24] Automated, data-driven methods are required for reliable, reproducible, and user-independent analyses.

The analysis of impedance spectra using the distribution of relaxation times is an alternative method for determining polarization contributions at a given number of time constants. In this method, RC circuits serve as a kernel function for resistive-capacitive processes.[25] Distributed processes and non-linearities are described by distribution functions of the kernel function over preset time constants. The distribution function is the ensemble of a finite number of polarization contributions $h(\tau_i) = R_i$ at each time constant τ_i. To additionally determine serial, lumped elements without characteristic time constants, such as ohmic resistance, inductance, and capacitance, the method was expanded to the extended DRT (eDRT) in Hahn et al.[26] With the generalized DRT (gDRT), resistive-inductive processes with their

characteristic time constants can also be examined.[27] The DRT analysis is an already well-established technique with a growing scientific base.[13] It works without strong model assumptions and covers the most relevant types of processes. Its main advantage is the separation of processes with overlapping ranges of time constants, which cannot be easily separated using classical EIS analysis techniques.[27] The main criticism is the required regularization.[6,13,28] To identify the polarization contributions, a linear optimization problem is solved. The optimization problem is ill-conditioned and ill-posed and hence requires regularization.[27,28] Regularization adds penalty terms to the objective function, which adjusts the optimization problem, resulting in a mathematically unique solution and a smoothing of the distribution function. In most cases, a variant of the Tikhonov regularization is applied.[29–32] The regularization parameter λ adds a degree of freedom to the determination of the distribution function. An automated selection of λ[33,34,30] can be used to achieve meaningful and reproducible DRT results.

The Loewner method (LM) introduced in Rüther et al.[28] offers a data-driven and regularization-free approach to determine the transfer functions of batteries. Instead of solving an optimization problem, the LM, as proposed by Mayo and Antoulas,[35] follows a purely interpolatory approach. LM is based on the systems theory of linear, time-invariant systems. The resulting model order is equal to the number of data points used and can be reduced by a singular value decomposition of the Loewner matrices.[35–37] As the Loewner matrices are defined for frequency response data, a direct feedthrough, e.g., for an ohmic resistance, is not taken into account. Ultimately, LM provides characteristic time constants and gains by interpreting the generalized eigenvalues of the system matrices that are calculated by feeding split datasets into the Loewner matrices.[28,38] The primary benefit of LM is that it does not require regularization, meaning that the distribution function is a unique solution and yet less smoothed. When used for impedance analysis, it yields a sharper separation of processes based on their characteristic time constants compared to the DRT analysis and provides a reliable quantification of polarization contributions.[6] Similar to the DRT, LM operates without strong model assumptions.[6,28] It only requires kernel functions to assign eigenvalues to specific transfer functions. However, identifying and interpreting serial, lumped elements as well as resistive-inductive processes remains challenging.[6,28] Furthermore, the absence of regularization can impede the interpretation of state variations or noise, as the corresponding effects are not smoothed. Determining the minimal model order is not straightforward and is therefore a degree of freedom in system identification, which can lead to overfitting or systematic model errors.

Consequently, the objective of this publication is to develop a method for impedance data analysis that meets the above requirements and combines the advantages of the generalized DRT analysis and the Loewner method while addressing the criticism raised.

RESULTS

Methods for ELSA

System identification using the ELSA is structured in five parts:

(1) the full-order linear time-invariant (LTI) state-space description from impedance data using the Loewner method,
(2) the conversion of the state-space description into a transfer function,
(3) the model order reduction,

(4) the calculation of the distribution of relaxation times and the minimal state-space description, and

(5) the final system analysis.

Full-order LTI state-space description from impedance data

During impedance measurements, electrochemical systems function as a single input-single output (SISO) system. In the galvanostatic mode, current is the input $u(t) = I(t)$ and voltage is the system response $y(t) = U(t)$. Applying the Loewner method[28] to impedance data comprises the main steps of data splitting, assigning the data to Loewner pencils, and identifying LTI state-space matrices of a SISO system, E_L, A_L, B_L, and C_L. These constitute the system equation

$$E_L \, \dot{x}(t) = A_L \, x(t) + B_L \, u(t) \qquad \text{(Equation 1)}$$

and the output equation

$$y(t) = C_L \, x(t). \qquad \text{(Equation 2)}$$

The latter is noted without a feedthrough matrix, i.e., $D_L = 0$. Eventually occurring direct feedthrough will be included as an algebraic equation in the system equation through a zero row in the singular mass matrix E_L, making it a differential-algebraic system. In general, the Loewner method yields a system with a number of state variables, and thus the full system order, equal to the number of measured frequencies $n = \dim(x) = N_f$. Accordingly, the dimensions of the system matrices are $\dim(A_L) = \dim(E_L) = n \times n$, $\dim(B_L) = n \times 1$, and $\dim(C_L) = 1 \times n$. For a comprehensive explanation of the Loewner framework and the calculation of the state-space matrices, please refer to Note S1 and Rüther et al.,[28] Gosea et al.,[36] Antoulas et al.,[39] and Antoulas et al.[40]

Conversion of state-space description to transfer function

To avoid the symbolic inversion of the textbook calculation of the SISO transfer function in the Laplace domain

$$G_L(s) = C_L \cdot (sE_L - A_L)^{-1} \cdot B_L, \qquad \text{(Equation 3)}$$

zeros and poles can be calculated separately. The poles β are determined by the generalized eigenvalues of A_L incorporating E_L. The zeros α are resolved through the extended system matrix $A_{L,ext}$ incorporating $E_{L,ext}$, where $E_{L,ext} = \begin{bmatrix} E_L & 0 \\ 0 & 0 \end{bmatrix}$ and $A_{L,ext} = \begin{bmatrix} A_L & B_L \\ C_L & D_L \end{bmatrix}$. The static gain is given by $k = G(s = 0) = C \cdot (-A)^{-1} \cdot B$ resulting in the product form of the transfer function

$$G_L(s) = k \cdot \frac{\prod_{i=1}^{N_{L,z}} (s - \alpha_i)}{\prod_{i=1}^{N_{L,p}} (s - \beta_i)}, \qquad \text{(Equation 4)}$$

with $N_{L,z}$ zeros $\alpha_i \in \mathbb{C}$ and $N_{L,p}$ poles $\beta_i \in \mathbb{C}$ and the model order $n = \max\{N_{L,z}, N_{L,p}\}$. The expansion of the products yields the polynomial form of the transfer function. Provided that the system is stable, the transfer function in the Laplace domain can be converted into the impedance function

$$Z_L(j\omega) = \frac{U(j\omega)}{I(j\omega)} = G_L(s)\big|_{s=j\omega}. \qquad \text{(Equation 5)}$$
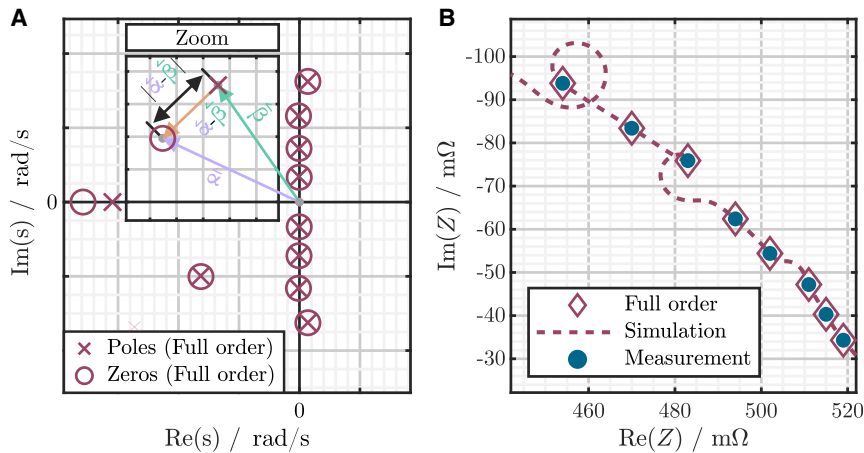
Figure 1. Model order reduction and overfitting
(A) Schematic representation of the model order reduction as noted in Equation 8.
(B) Zoom into an impedance spectrum of a redox flow battery. The simulated spectrum is shown at an intermediate frequency point for an overdetermined model order.

If more zeros than poles appear, i.e., $N_{L,z} > N_{L,p}$, then a number of $N_\infty = N_{L,z} - N_{L,p}$ zeros occur at infinity. In the numerical calculation of Equation 4, these may appear as extremely large values of $|\alpha_i|$ and can therefore be deleted.

Model order reduction

In impedance-based analysis of electrochemical systems, it is common to have a greater number of frequency measurement points than the system order, resulting in an overdetermined system of equations. This leads to a state-space description using the Loewner method with a system order of $n = N_f$, which yields minimal residuals but may show signs of overfitting. Overfitting can be recognized when calculating the impedance function (Equation 5) at intermediate frequency points. Results may include impedance loops that cannot be attributed to the system under investigation, as exemplified in Figure 1B. To quantitatively measure overfitting, the Euclidean norm of the curvature $\|\kappa(Z(j\omega_{of}))\|_2$ of the modeled impedance in the complex plane at frequency points ω_{of} different from the measured ones can be used.[41] The detailed definition of the curvature can be found in the Note S2. To obtain a system description without overfitting and with minimal size (i.e., a model order $r < n$), model order reduction is required. To ensure reproducible impedance analysis, model order reduction should not be a degree of freedom but rather an automated process step. Instead of singular value decomposition in the Loewner method, in ELSA, the model order reduction follows a systems-theoretical approach by canceling equal poles and zeros, $\alpha_i = \beta_j$, in the transfer function (Equation 4). This leads to the reduced transfer function

$$G_{red}(s) = k \cdot \frac{\prod_{i=1}^{N_z} (s - \alpha_i)}{\prod_{i=1}^{N_p} (s - \beta_i)} \qquad \text{(Equation 6)}$$

and the reduced impedance function

$$Z_{red}(j\omega) = G_{red}(s)\big|_{s = j\omega}, \qquad \text{(Equation 7)}$$
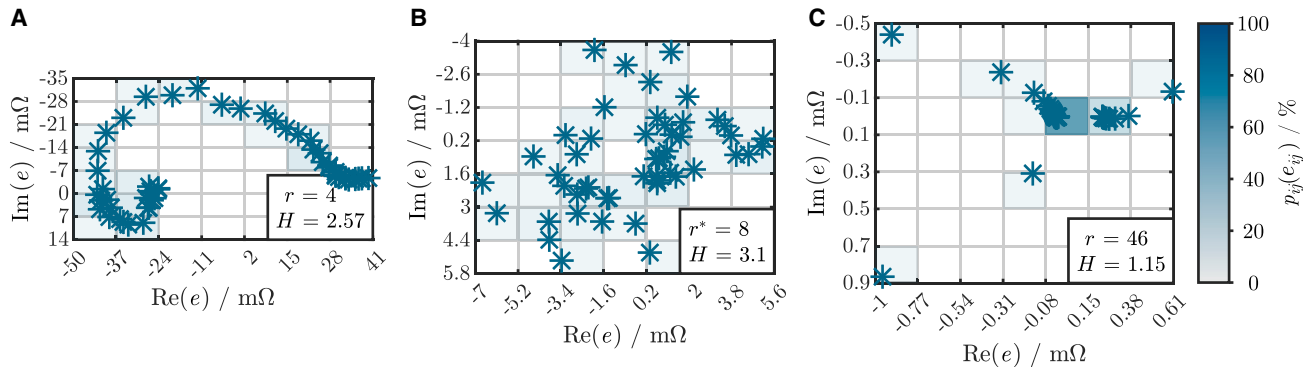
Figure 2. Shannon entropy of impedance residuals
(A–C) Calculation of the Shannon entropy by the complex residual of the measured and modeled impedance spectra of a redox flow battery for a (A) low, (B) minimal, and (C) high model order.

with $N_z < N_{L,z}$ and $N_p < N_{L,p}$ and the model order $r = \max\{N_z, N_p\}$. Since the calculated poles and zeros will numerically not precisely match, the equality condition can be weakened to $\alpha_i \approx \beta_j$ with

$$\frac{|\alpha_i - \beta_j|}{|\beta_j|} < \varepsilon_{\text{red}}, \qquad \text{(Equation 8)}$$

as illustrated in Figure 1A.

The variable threshold ε_{red} is selected to ensure that the reduced impedance function still accurately describes the impedance data, resulting in a low sum of squared errors

$$sse = \sum_{i=1}^{N_f} \left(\text{Re}\{Z_{\text{meas}}(j\omega_i) - Z_{\text{red}}(j\omega_i)\}^2 + \text{Im}\{Z_{\text{meas}}(j\omega_i) - Z_{\text{red}}(j\omega_i)\}^2 \right) \quad \text{(Equation 9)}$$

without overfitting. The latter can be achieved by selecting model orders with low norms of the curvature $\|\kappa\|$ in the Nyquist plot. Systematic errors,[41] i.e., residuals that show a functional dependency as depicted in Figure 2A, can be excluded by analyzing the Shannon entropy[42]

$$H = - \sum_{i=1}^{N_f} p(e(j\omega_i)) \cdot \log\{p(e(j\omega_i))\}, \qquad \text{(Equation 10)}$$

with the probability $p \in [0, 1]$ of the residual $e(j\omega_i) = Z_{\text{meas}}(j\omega_i) - Z_{\text{red}}(j\omega_i)$. The Shannon entropy of the residual is calculated using the relative frequency of $e(j\omega_i)$ in a range in the complex plane, which is subdivided into N_{bin}^2 evenly distributed bins. A grid is formed by N_{bin} bins for both the real and imaginary parts, covering the range between the maximum and minimum real and imaginary residuals, as depicted in Figure 2. For high model orders, the small residuals display a distinct center of gravity in Figure 2C, with single outliers resulting in a low Shannon entropy. For low model orders in Figure 2A, the large residuals exhibit a systematic pattern that also leads to a low Shannon entropy. If the residuals deviate significantly from white noise, then they carry relevant information that could be modeled by a model extension, i.e., a higher order model.[43] Only for the correct model order do the residuals show a homogeneous distribution, seen in Figure 2B, resulting in a maximum Shannon entropy.

A variation of the threshold ε_{red} and the resulting model order r, as presented for each impedance spectrum analyzed, exhibit a unique solution for the minimal
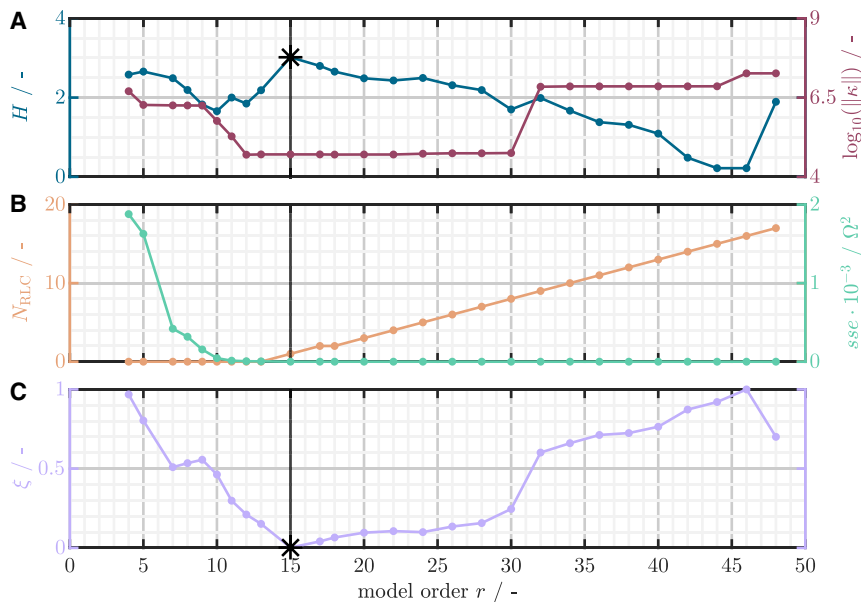
Figure 3. Selection of minimal model order for a lithium-ion cell
(A and C) Selection of minimal model order for a cylindrical LFP | graphite cell by (A) norm of curvature κ and Shannon entropy H, and (C) search function ξ.
(B) Sum of squared errors sse and number of RLC elements N_{RLC}.

resulting order of the reduced impedance function. The minimal model order r^* is found in a range of low values of the norm of the curvature $\|\kappa\|$ where the Shannon entropy H is high, and the squared error sse is still low, as exemplarily shown for a lithium-ion battery impedance spectrum in Figures 3A and 3B. The automated and unique determination of the minimal model order r^* is conducted by a minimum search of the function

$$\xi(r) = \text{mmn}(\text{mmn}(sse(r)) + \text{mmn}(\|\kappa(r)\|) + \text{mmn}(-H(r))), \quad \text{(Equation 11)}$$

where ξ is the normalized linear combination of the normalized sse, the normalized $\|\kappa\|$, and the normalized negative entropy H, using the min-max normalizing function $\text{mmn}(x) = (x - \min(x)) \cdot (\max(x) - \min(x))^{-1}$ for a data vector x. Furthermore, it is possible to consider weighted or non-linear combinations for the selection function. Figure 3C exemplarily shows ξ as a function of the model order r. A model order determined in this way fulfills the requirements of high precision and minimal order without overfitting.

DRT and minimal state-space description
By partial fraction expansion, the transfer function (Equation 6) can be expanded to

$$G_{red}(s) = R_0 + sL_0 + \frac{1}{sC_0} + \sum_{i=1}^{N_{real}} \frac{\gamma_i}{s - \beta_i} + \sum_{i=1}^{N_{cc}} \left(\frac{\delta_i + j\varepsilon_i}{s - (\lambda_i + j\mu_i)} + \frac{\delta_i - j\varepsilon_i}{s - (\lambda_i - j\mu_i)} \right),$$
(Equation 12)

with N_{real} real single poles and N_{cc} pairs of conjugate complex poles.[44] If the number of zeros N_z exceeds the number of poles N_p in Equation 6, then a polynomial term in s occurs. The constant and the linear element can immediately be recognized as ohmic resistance R_0 and inductivity L_0. Differences of $N_z - N_p > 2$ are ignored here. A single real valued pole in the origin can directly be assigned to a capacitance

C_0. All three elementary transfer functions of R_0, L_0, and C_0 do not carry characteristic time constants, occur as summands in Equation 12, and are hence serial, lumped elements of the DRT. The summands of the real single poles in Equation 12 have the mathematical structure of a PT1 element $-\gamma_i/\beta_i/1 - s/\beta_i|_{s=j\omega} = \frac{a}{1+j\omega\,b}$. The signs of the parameters a and b can be positive or negative. For all combinations of a and b, a case differentiation of single poles is discussed in Note S4 and Figure S1. Only for case 1 with positive values, $a > 0$ and $b > 0$, is a physical interpretation of an RC circuit

$$Z_{RC}(j\omega) = \frac{a}{1+j\omega\,b} = \frac{R}{1+j\omega\,\tau} \qquad \text{(Equation 13)}$$

with passive components for $a = R$ and $b = \tau = R \cdot C$ immediately possible. For case 2 with $a < 0$ and $b > 0$, the elementary transfer function of the PT1 element can be rearranged to a serial connection of a P element and a DT1 element, i.e., the impedance of a parallel RL circuit

$$Z_{RL}(j\omega) = \frac{-|a|}{1+j\omega\,b} = -R + \frac{j\omega\,R\,\tau}{1+j\omega\,\tau}, \qquad \text{(Equation 14)}$$

with $R = |a|$ and $\tau = L/R = b$, cf. Equation S13. The serial resistance corrects the ohmic resistance in Equation 12. Rarely occurring summands of real single poles in Equation 12 with negative time constants,[45,46] i.e., $b < 0$, indicate an active element, a non-linearity, or time variance in the impedance data. For case 3 with $a > 0$ and $b < 0$, the element shows resistive-inductive behavior with positive imaginary parts. Accordingly, for case 4 with $a < 0$ and $b < 0$, the element shows resistive-capacitive behavior with negative imaginary parts only.

The impedance functions of the conjugate complex pole pairs in Equation 12 are

$$Z_{ccp,i}(j\omega) = \left.\frac{\frac{(\delta_i+j\varepsilon_i)}{(-(\lambda_i+j\mu_i))}}{1 - \frac{s}{(-(\lambda_i+j\mu_i))}}\right|_{s=j\omega} = \frac{a+jb}{1+j\omega\,(c+jd)} \qquad \text{(Equation 15)}$$

and

$$Z_{ccn,i}(j\omega) = \left.\frac{\frac{(\delta_i - j\varepsilon_i)}{(-(\lambda_i - j\mu_i))}}{1 + \frac{s}{(-(\lambda_i - j\mu_i))}}\right|_{s=j\omega} = \frac{a - jb}{1+j\omega\,(c - jd)}. \qquad \text{(Equation 16)}$$

In systems theory, conjugate complex pole pairs represent resonant signals or systems. A real resonant circuit consists of a capacitance C in parallel to an inductivity L and an ohmic resistance R in the inductive path and is described by the impedance function

$$Z_{RLC}(j\omega) = \frac{R+j\omega\,L}{1+j\omega\,CR - \omega^2\,LC}. \qquad \text{(Equation 17)}$$

The combined impedance functions of the conjugate complex pole pairs are equal to the impedance function of the RLC circuit if $R = 2a$, $L = 2ac - 2bd$, and $C = c/a$.[47]

Single pole transfer functions with time constants (far) outside the measured frequency range can be reinterpreted as serial, lumped elements, i.e., by a resistance R, an inductance L, or a capacitance C, by considering the limiting behavior of their impedance equation as derived in Note S5 and listed in Table S1.

The resulting impedance function of the ELSA

$$Z_{ELSA}(j\omega) = \frac{U(j\omega)}{I(j\omega)} = Z_R + Z_L(j\omega) + Z_C(j\omega) + \sum_{i=1}^{N_{RC}} Z_{RC,i}(j\omega) + \sum_{i=1}^{N_{RL}} Z_{RL,i}(j\omega)$$

$$+ \sum_{i=1}^{N_{RLC}} Z_{RLC,i}(j\omega) = R_0 + j\omega\, L_0 + \frac{1}{j\omega\, C_0} + \sum_{i=1}^{N_{RC}} \frac{R_i}{1 + j\omega\, \tau_i}$$

$$+ \sum_{l=1}^{N_{RL}} \frac{j\omega\, R_l\, \tau_l}{1 + j\omega\, \tau_l} + \sum_{k=1}^{N_{RLC}} \frac{R_k + j\omega\, L_k}{1 + j\omega\, C_k R_k - \omega^2 C_k L_k} \qquad \text{(Equation 18)}$$

comprises serial, lumped elements, ohmic resistance, inductance, and capacitance, as well as discrete distributions of impedance functions with characteristic time constants for the resistive-capacitive behavior, $Z_{RC}(j\omega)$, and for resistive-inductive behavior, $Z_{RL}(j\omega)$. Additionally, it covers resonant processes $Z_{RLC}(j\omega)$. In most cases, $Z_{ELSA}(j\omega)$ contains passive elements with positive parameters, i.e., R, L, and C, only. In case negative time constants occur, active elements, non-linearities, and time variance need to be discussed.

The reduced and interpreted impedance function (Equation 18) can be transformed back into a minimal state-space representation with the current as input $u(t) = I(t)$ and the terminal voltage as output $y(t) = U(t)$.

$$\dot{x}(t) = A\, x(t) + B\, u(t) \qquad \text{(Equation 19)}$$

$$y(t) = C\, x(t) + D\, u(t) \qquad \text{(Equation 20)}$$

The system equation of this LTI system has minimal order, i.e., $r^* = \dim(x) \leq n$. Here, it is exemplarily shown for a restive-capacitive system with an ohmic resistance R and N_{RC} RC elements with the voltages of each parallel circuit as state variables:

$$x = \left[U_{RC,1} \cdots U_{RC,N_{RC}} \right]^T, \qquad \text{(Equation 21)}$$

$$\dot{x}(t) = \begin{bmatrix} -\tau_1^{-1} & \cdots & 0 \\ \vdots & \ddots & \vdots \\ 0 & \cdots & -\tau_{N_{RC}}^{-1} \end{bmatrix} x(t) + \begin{bmatrix} R_1/\tau_1 \\ \vdots \\ R_{N_{RC}}/\tau_{N_{RC}} \end{bmatrix} u(t), \text{and} \qquad \text{(Equation 22)}$$

$$y(t) = [1 \cdots 1]\, x(t) + R \cdot u(t). \qquad \text{(Equation 23)}$$

System analysis

The identified system is described by different mathematical representations: in the Laplace domain as a transfer function in polynomial and in product form (Equation 6), in the frequency domain as the impedance function (Equation 18), and in the time domain as a state-space representation (Equations 22 and 23). Graphical representations contain the same information and include a pole-zero plot, Nyquist plot, Bode plot, and DRT plot. The distribution of relaxation times plot displays the distributed polarization contributions $h(\tau)$ at their specific time constants: resistive-capacitive behavior of RC elements in the positive and resistive-inductive behavior of RL elements with a given negative sign in the negative half-plane. The resonant behavior of RLC elements is depicted with Dirac impulses in both half-planes at the characteristic time constant τ_{RLC} where the RLC circuit has its maximum amplitude $|h_{RLC}|$.[47] All mathematical and graphical representations of the identified system using ELSA have advantages for interpreting and discussing measured impedance spectra.
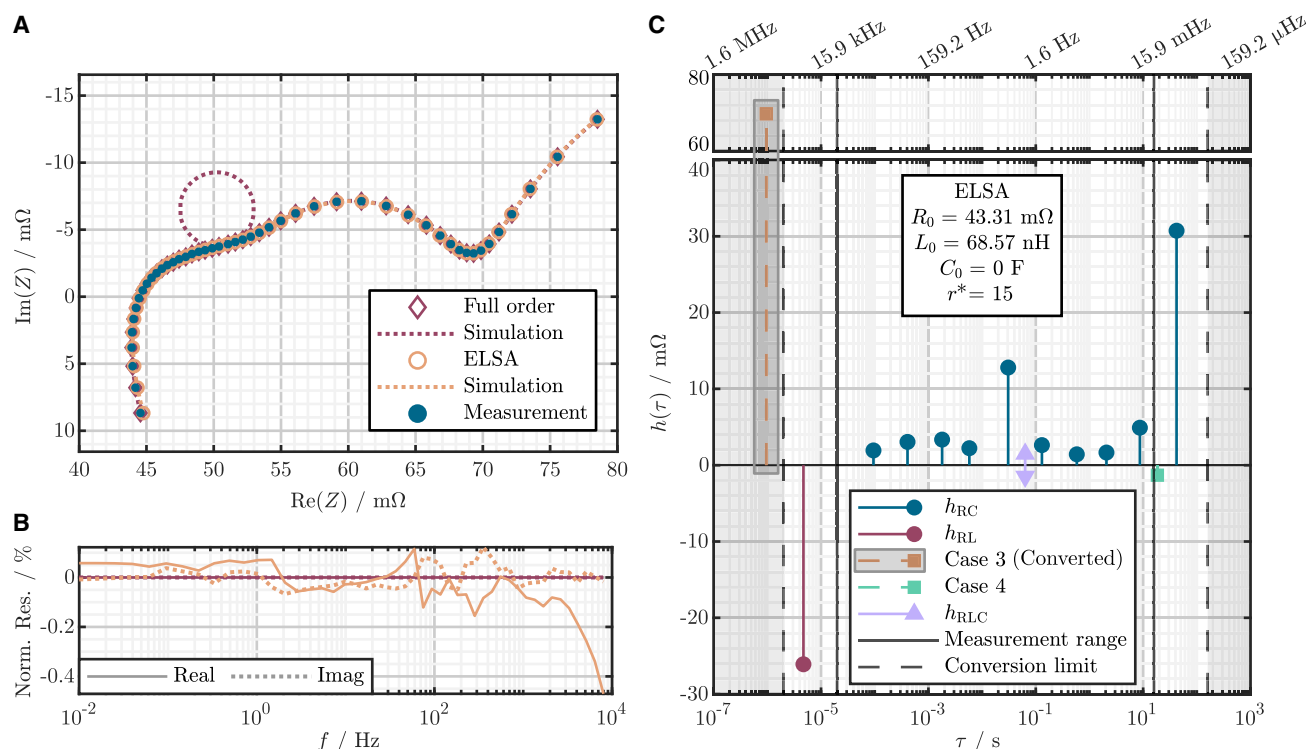
Figure 4. ELSA results of a lithium-ion cell

Analysis results of a cylindrical LFP | graphite cell from A123 Systems.

(A) Nyquist plot of measured and simulated impedance spectra, (B) normalized residuals, and (C) distribution of polarization for RC, RL, and RLC elements with identified serial, lumped elements.

Results of the analysis

Results of the ELSA are presented for different electrochemical systems including lithium-ion batteries, polymer electrolyte membrane (PEM) fuel cells, a redox flow battery, and a double-layer capacitor. Additionally, the ELSA algorithm's capability is demonstrated by investigating an analog circuit with known circuit element parameters. For all analyzed spectra, the model reduction was calculated using the same threshold values of Equation 8 in the range of $\varepsilon_{\text{red}} \in [1 \cdot 10^{-6}, 1 \cdot 10^{-1}]$. To test for overfitting, the curvature was calculated using 50,000 logarithmically spaced frequency points between the minimum and maximum measured frequencies of each spectrum. The test can also be performed with fewer frequency points, but the impedance loops may be less visible.

Lithium-ion battery

The impedance spectrum shown in Figure 4A is derived from a cylindrical 26650 lithium iron phosphate | graphite cell manufactured by A123 Systems with a nominal capacity of 2.5 Ah.[27] Figure 3 displays the outcomes of the model order reduction. Varying ε_{red} in the given range produces model orders ranging from 4 to 48. Figure 3A shows the norm of the curvature of the resulting impedance spectra and the Shannon entropy of the resulting complex residuals as a function of the model order. At a model order of $r^* = 15$, a unique maximum of the Shannon entropy can be found in the range of low curvature norms. Figure 3B depicts the low error at the found optimum. The number of RLC elements is still 1 at the entropy maximum. Figure 3C displays the search function ξ for the automated and unique determination of the minimal model order.

Figure 4A shows the Nyquist plot of the measured and simulated spectra, including the full- and minimal order models, both with simulation results at intermediate frequencies. The dotted impedance loop of the full-order spectrum at an intermediate frequency point clearly indicates overfitting. The distributed polarization contributions $h(\tau)$ for RC, RL, and RLC elements at their specific time constants are shown in Figure 4C: a single RL circuit for the resistive-inductive high-frequency tail and a distribution of ten RC circuits for the resistive-capacitive impedance arches and the diffusive impedance tail. The remaining RLC element at medium frequencies in proximity to the large Dirac pulse and the case 4 element at low frequencies indicate that the measured impedance spectrum contains hints of nonlinearity or time variance. An identified element of case 3 with a time constant more than a decade below the measured frequency range is converted into a serial ohmic resistance and an inductance according to Table S2. The resulting values of R_0, L_0, and C_0 can be found in Figure 4C. Overall, the ELSA spectrum precisely describes the measured impedance data without overfitting. The low normalized residuals in Figure 4B indicate a slight increase in the real part for high frequencies, which originates from the conversion of the case 3 element. The high accuracy over the wide frequency range is also evident in the Bode plot in Note S6 and Figure S2. The pole-zero plot of the final ELSA spectrum in Figure S2B comprises 14 poles and 15 zeros. All poles and zeros are located in the left half-plane. Two of each form conjugate pole pairs that are responsible for the RLC element. The model order is determined by the maximum number of zeros or poles, $r = \max\{N_z, N_p\} = 15$. This number is equal to the number of DRT elements, $r = N_{RC} + N_{RL} + 2N_{RLC} + N_{case3} + N_{case4} = 15$. The conversion of a case 3 element into a resistance and an inductance reduces the number of poles by one, increases the number of zeros by one, and keeps the model order constant.

Vanadium redox flow battery

The impedance spectrum of the vanadium redox flow battery in Figure 6A was published by Schneider et al.[48] and examined using the gDRT analysis in Danzer.[27]

The model order reduction shown in Figure 5 provides a unique solution for a minimal model order of 8. The reduced impedance model precisely describes the measured spectrum across the entire frequency range, as depicted in Figures 6A and 6B. The impedance loops at intermediate frequency points clearly indicate the overfitting of the full-order model. ELSA results of the spectrum reveal an ohmic resistance, an inductance, five RC circuits, and an RLC circuit but no RL circuit. The results partially differ from the gDRT analysis in Danzer.[27]

Figure 7 compares the calculated DRT of gDRT and ELSA, showing a high level of agreement between both distribution functions, the Dirac pulses of ELSA, and the peaks of gDRT. However, three significant differences were observed. First, at large time constants, gDRT incorrectly finds an RC and an RL circuit, whereas ELSA identifies an RLC circuit. Second, due to the incorrectly found RL peak at low time constants, the ohmic resistance is offset by about 40 mΩ. Third, gDRT finds four resistive-capacitive peaks (nos. 1–4 in gray in Figure 7) within the range $\tau \in [10\ \mu s$, 100 ms], while ELSA identifies five characteristic time constants (nos. 1–5 in blue in Figure 7). The two closely spaced but separated Dirac pulses (nos. 3 and 4) of the ELSA DRT get combined in the gDRT analysis to form the single dominant peak 3 as a result of the Tikhonov regularization.
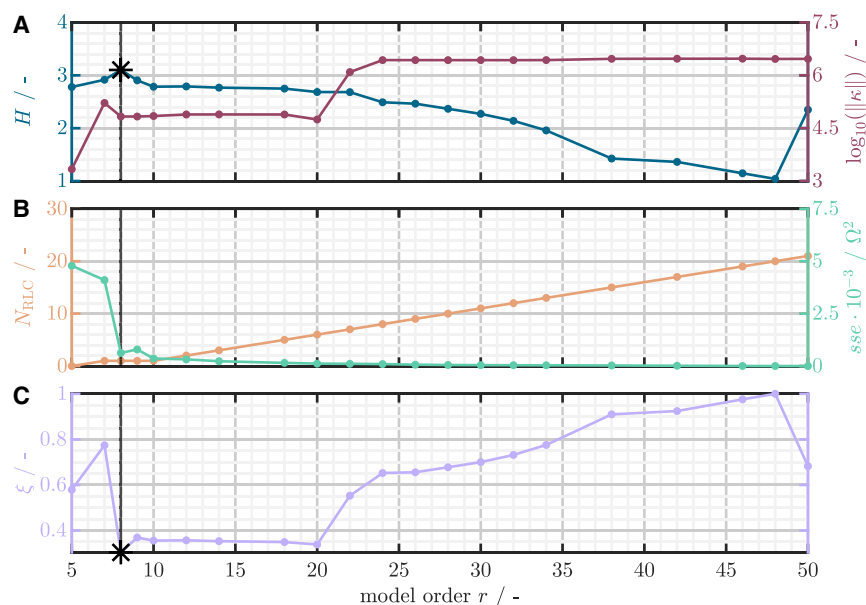
Figure 5. Selection of minimal model order for a redox flow battery
(A and C) Selection of minimal model order for a vanadium redox flow battery by (A) norm of curvature κ and Shannon entropy H and (C) search function ξ.
(B) Sum of squared errors sse and number of RLC elements N_{RLC}.

PEM fuel cell

The impedance spectrum of a PEM fuel cell[49] in Figure 9A shows a pronounced resistive-inductive behavior at low frequencies and already optically recognizable noise.

The ELSA DRT in Figure 9C shows four resistive-capacitive RC elements; two RL elements, each with characteristic time constants; and a series of RLC elements across the measured frequency range. The occurrence of measurement noise correlates with the occurrence of RLC elements in ELSA. The model reduction yields a unique minimum of the search function ξ at a model order of 17, as shown in black in Figure 8C. The search function ξ shows a local minimum at a lower model order of 13 (in gray), shortly before the sse increases drastically. In this particular case, it would be justified to select the lower model order and cancel two more RLC elements (light purple in Figure 9C) that are attributable to measurement noise. It is noteworthy that the removal of elements does not influence the time constants of other identified polarization contributions. The quality of impedance analysis, no matter which method is used, heavily depends on the quality of the impedance measurement and hence a proper selection of test conditions.

NMC-graphite lithium-ion battery, double-layer capacitor, high-temperature PEM, and analog RLC circuit

To further demonstrate the working principle and versatility of the ELSA, additional spectra of a nickel manganese cobalt oxide (NMC)-graphite lithium-ion battery,[50] a double-layer capacitor,[27] a high-temperature PEM,[51] and an analog RLC circuit have been examined. The results can be found in Note S7.

DISCUSSION

The ELSA is based on the data-driven, interpolatory Loewner method, which avoids making strong model assumptions. ELSA identifies model elements and characteristic parameters for all (electrochemical) systems analyzed, including those in the
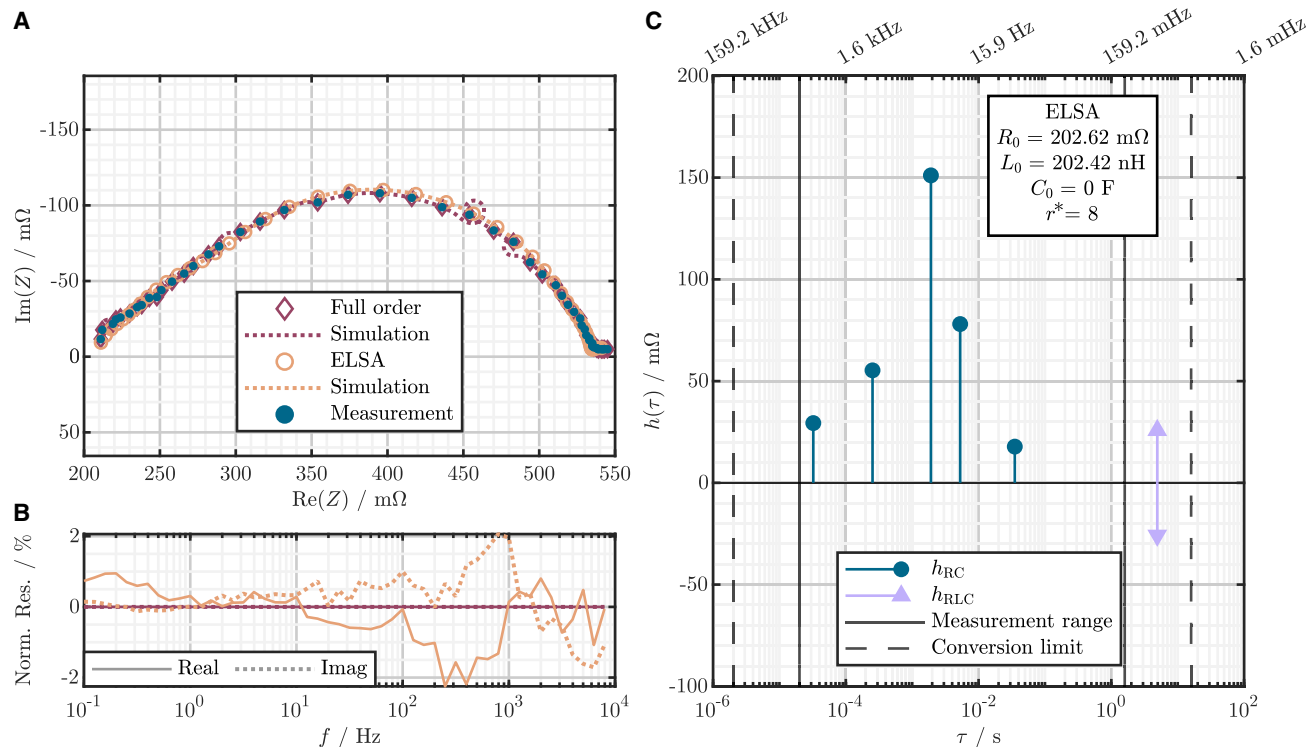
Figure 6. ELSA results of a vanadium redox flow battery
Analysis results of a vanadium redox flow battery.
(A–C) (A) Nyquist plot of measured and simulated impedance spectrum, (B) normalized residuals of the measured and reduced impedance spectra, and (C) distribution of polarization for RC and RLC elements.

supplemental information, to accurately describe the given impedance data. Model order reduction, based on canceling equal or close zeros and poles in the identified transfer function, results in a reliable and robust determination of the minimal model order. To avoid both overfitting and systematic errors, the curvature of the locus and the Shannon entropy of the complex residuals are used. The resulting linear state-space description is of minimal order. ELSA identifies impedance models that consist of parameters with physical interpretability, i.e., positive parameters for passive systems, R_0, L_0, and C_0 as serial, lumped elements, distributions of RC and RL elements for resistive-capacitive and resistive-inductive behavior, and RLC elements for resonant processes. Occasionally occurring elements with a negative time constant indicate non-linearities and time variance in the measured impedance spectra, requiring further analysis.

Besides the discussion of single impedance spectra analyzed, the working principle of the ELSA shall be discussed in comparison and in differentiation to the Loewner method and the generalized distribution of relaxation times analysis.

In LM, the full-order transfer function generated with $n = N_f$ is reduced in order by compressing the Loewner matrices using projection matrices based on a singular value decomposition to extract the dominant features.[6,13,28] In contrast, ELSA adopts a systems-theoretical approach for model order reduction by canceling equal or close zeros and poles. The determination of the model order in LM can be ambiguous when dealing with distributed processes or measurement noise due to the use of singular values. Therefore, approximations must be used.[28] On
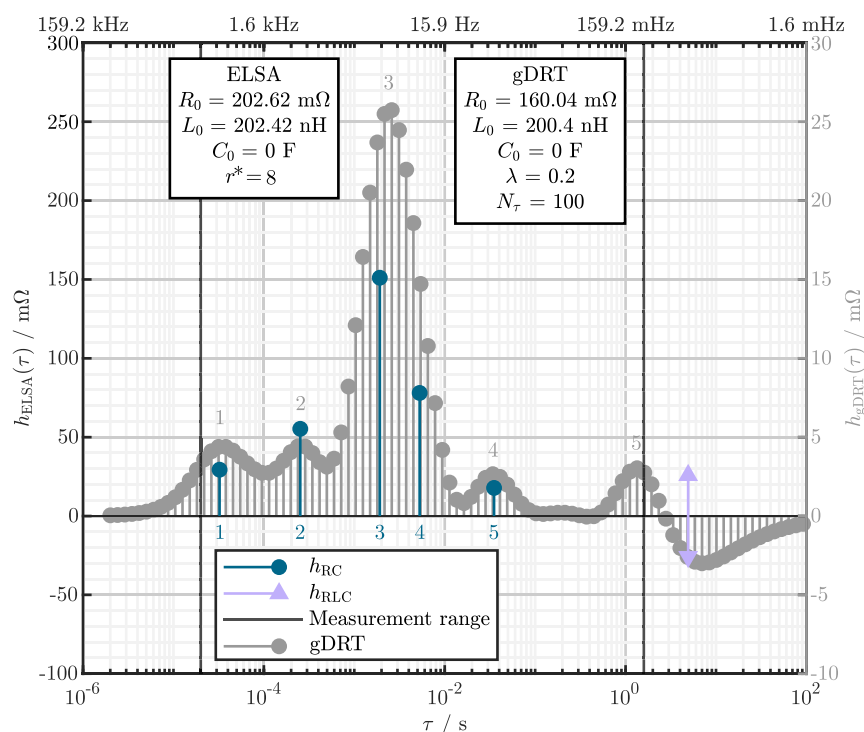
Figure 7. Comparison of distributed polarizations

Comparison of distributed polarization of a vanadium redox flow battery identified by gDRT and ELSA.

the other hand, ELSA uses a combination of different evaluation measures, Shannon entropy, curvature, and sum of squared errors, which leads to an unambiguous and automated determination of the minimal model order without further degrees of freedom. The conventional LM determines the distribution function through eigenvalue decomposition, which restricts the analysis to RC circuits. These elements appear as Jordan blocks, from which lumped elements can be calculated.[28] However, this approach is challenging, and Jordan blocks can include several lumped or RL elements. In contrast, ELSA allows for the calculation of not only RC and serial, lumped elements but also RL and RLC elements.

In contrast to gDRT, ELSA does not require the solution of an optimization problem. More importantly, it does not require regularization. The smoothing effect of regularization hinders the separation of close time constants and the disentanglement of processes, as shown for the redox flow battery. Furthermore, regularization occasionally leads to artifacts in the distribution function that cannot be attributed to physical processes, as demonstrated for the PEM and the high-temperature PEM (in the supplemental information). Therefore, by using ELSA, the interpretation of underlying processes is not "lost in regularization." The model order of gDRT is set by the predefined vector of time constants, which is typically two or three times the number of measured frequencies. In gDRT, model order reduction is not explicitly carried out, resulting in a distribution of polarization that may not be of minimal order. However, certain frequencies may exhibit zero gains. The exact characteristic time constants cannot be identified due to the preset fixed values of the time constants. Even with the addition of RL and serial, lumped elements to the DRT, gDRT does not allow for the identification of resonant processes.
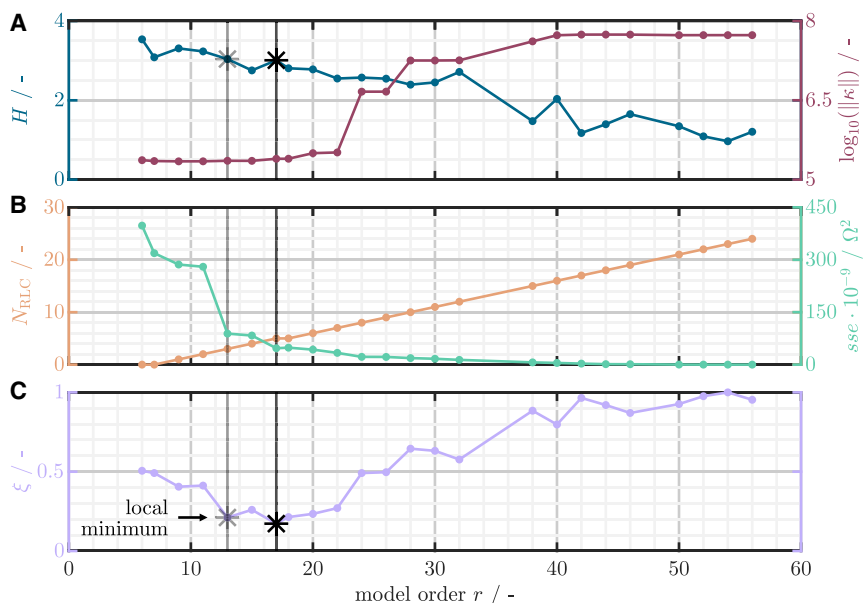
Figure 8. Selection of minimal model order for a PEM fuel cell
(A and C) Selection of minimal model order for a PEM fuel cell by (A) norm of curvature κ and Shannon entropy H and (C) search function ξ.
(B) Sum of squared errors sse and number of RLC elements N_{RLC}.

The ELSA follows a systems-theoretical approach to analyze impedance spectra of electrochemical systems at various levels, including material, component, cell, and system. Due to its general approach, ELSA can be applied to frequency domain data in various fields of application beyond electrochemistry. The embedded systems-theoretical method of model order reduction also qualifies ELSA for the reduction of complex physico-chemical impedance models for efficient simulation and engineering purposes. In the way ELSA identifies descriptive impedance models, it adopts the comprehensive analysis of the generalized distribution of relaxation time analysis. However, instead of model fitting, which involves solving an optimization problem, ELSA utilizes the data-driven, interpolatory approach of the Loewner method. This eliminates the need for regularization and thus avoids the major drawback of most DRT methods.

ELSA robustly and automatically finds models for given impedance data without making assumptions about the underlying physico-chemical processes or predefining model structures as equivalent-circuit approaches do. It provides a reliable method for determining the optimal balance between overfitting measured impedance spectra and oversimplifying with few expected model elements. The systems-theoretical approach employed for model order reduction as well as the analysis of the Shannon entropy of the complex residuals and the curvature of the locus enable a reproducible and automated determination of the minimal model order. This approach identifies the maximum number of observable system states that reflect the linear and time-invariant behavior of the system under investigation. Furthermore, ELSA enables the determination of an upper boundary for the maximum number of structurally identifiable parameters of an impedance spectrum, as demonstrated in Note S3 for a resistive-capacitive system.

ELSA identifies the largest set of model elements and elementary transfer functions for the DRT analysis of linear and time-invariant impedance spectra published
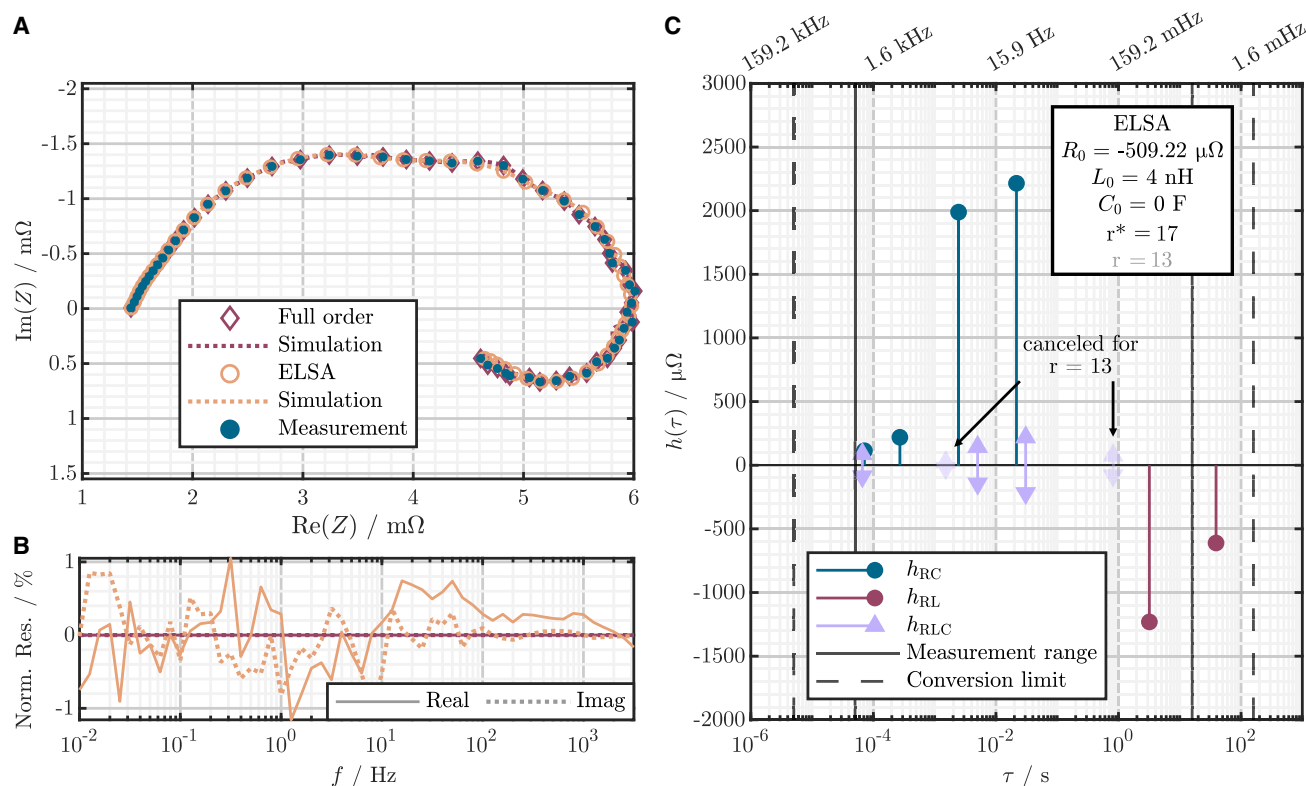
Figure 9. ELSA results of a PEM fuel cell

Analysis results of a PEM fuel cell.

(A) Nyquist plot of measured and simulated impedance spectrum, (B) normalized residuals of the measured and reduced impedance spectra, and (C) distribution of polarization for RC, RL, and RLC elements.

so far: lumped, serial elements (R_0, L_0, C_0), distribution functions for resistive-capacitive and resistive-inductive behavior (RC and RL elements), and resonant processes (RLC elements). This expands the method's potential applications beyond electrochemical systems, e.g., for circuit analysis as shown in Figure S11. ELSA has an additional benefit, as it enables the direct generation of an interpretable state-space representation by calculating transfer functions for each element.

According to the LTI systems theory on which ELSA is based, it focuses on linear, time-invariant impedance measurements. Although it does not include approaches to actively describe non-linearities and time variance, it can be used to analyze impedance data that do not meet LTI criteria. In such cases, ELSA identifies the LTI components of the analyzed spectra and determines the frequency range in which they occur. Furthermore, the remaining residuals, canceled elements of the model order reduction, as well as the identified RLC and single pole elements with negative time constants contain information on non-linearities, time variance, and noise. Hence, systematic errors, such as distortion, drift, and state variation, are detected by ELSA and identified as elements with low gains. With an in-depth analysis of these elements, further interpretation of systematic errors may be possible. Particularly for resonant systems, ELSA offers a novel and unique solution for testing the validity and LTI criteria of measured spectra. For these, well-established methods such as the linear Kramers-Kronig test[52] and Z-HIT[53] fail.

Table 1. Information on test objects, operating conditions, measurement equipment, and conditions as well as references

	Lithium-ion battery	Vanadium redox flow battery	PEM fuel cell
Technology details	A123 Systems, 26650 lithium iron phosphate | graphite, 2.5 Ah	microflow cell (Electrocell A/S, Tarm, DK), surface 10 cm^2	ElringKlinger single PEM fuel cell, active surface area 50 cm^2
Operating point	50% state of charge, 3.27 V, 20°C	50% state of charge, 1:4 V	1 A, relative humidity of 83.4%, stoichiometry of 4.0/2.0
Potentiostat/frequency response analyzer	Zahner Zennium Pro	Scribner 857, Gamry Reference 3000	Scribner Associates fuel cell test station with 885 Fuel Cell Potentiostat
EIS mode	galvanostatic	potentiostatic	galvanostatic
Amplitude	30 mA	10 mV	100 mA
Min. frequency (mHz)	52	100	10
Max. frequency (kHz)	17	10	3.981
No. of frequencies	49	51	57
Reference	Danzer[27]	Danzer[27] and Schneider et al.[48]	Pivac et al.[49]

In summary, ELSA offers a new foundation for the reproducible analysis and consistent interpretation of measured impedance spectra of electrochemical systems and beyond.

EXPERIMENTAL PROCEDURES

Resource availability

Lead contact

Further information and requests for resources should be directed to and will be fulfilled by the lead contact, Michael A. Danzer (danzer@uni-bayreuth.de).

Materials availability

The study did not generate unique materials.

Data and code availability

- All analyzed and generated datasets in this study are available from the lead contact without restriction. The datasets of the impedance spectra analyzed are available at Zenodo under https://doi.org/10.5281/zenodo.10794584.[54] The datasets of the analyses are available under https://doi.org/10.5281/zenodo.10794720.[55]
- All code used in this study is available at Zenodo under https://doi.org/10.5281/zenodo.11473099.[56]

Experiment summary

The experimental details and references to data sources and further analysis are shown in Table 1. Additional summaries of procedures can be found in the Notes S1–S7.

SUPPLEMENTAL INFORMATION

Supplemental information can be found online at https://doi.org/10.1016/j.xcrp.2024.102091.

ACKNOWLEDGMENTS

AUTHOR CONTRIBUTIONS

DECLARATION OF INTERESTS

REFERENCES

1. Schutter, B. (2000). Minimal state-space realization in linear system theory: an overview. J. Comput. Appl. Math. *121*, 331–354.

2. Kalman, R.E. (1960). On the general theory of control systems. IFAC Proc. Vol. *1*, 491–502.

3. Plett, G.L., and Trimboli, M.S. (2022). Process for lumping parameters to enable nondestructive parameter estimation for lithium-ion physics-based models. 35th International Electric Vehicle Symposium and Exhibition.

4. Bellman, R., and Åström, K.J. (1970). On structural identifiability. Math. Biosci. *7*, 329–339.

5. Kalman, R.E. (1963). Mathematical Description of Linear Dynamical Systems. Journal of the Society for Industrial and Applied Mathematics Series A Control *1*, 152–192.

6. Rüther, T., Schamel, M., Plank, C., Schomburg, F., Röder, F., and Danzer, M.A. (2023). Cell-to-cell variation beyond parameter analysis — Identification and correlation of processes in Lithium-Ion Batteries using a combined distribution of relaxation times analysis. J. Power Sources *587*, 233677.

7. Schuster, S.F., Brand, M.J., Berg, P., Gleissenberger, M., and Jossen, A. (2015). Lithium-ion cell-to-cell variation during battery electric vehicle operation. J. Power Sources *297*, 242–251.

8. Rüther, T., Plank, C., Schamel, M., and Danzer, M.A. (2023). Detection of inhomogeneities in serially connected lithium-ion batteries. Appl. Energy *332*, 120514.

9. Ranque, P., Gonzalo, E., Armand, M., and Shanmukaraj, D. (2023). Performance-based materials evaluation for Li batteries through impedance spectroscopy: a critical review. Mater. Today Energy *34*, 101283.

10. Galeotti, M., Cinà, L., Giammanco, C., Cordiner, S., and Di Carlo, A. (2015). Performance analysis and SOH (state of health) evaluation of lithium polymer batteries through electrochemical impedance spectroscopy. Energy *89*, 678–686.

11. Tang, Z., Huang, Q.-A., Wang, Y.-J., Zhang, F., Li, W., Li, A., Zhang, L., and Zhang, J. (2020). Recent progress in the use of electrochemical impedance spectroscopy for the measurement, monitoring, diagnosis and optimization of proton exchange membrane fuel cell performance. J. Power Sources *468*, 228361.

12. Rüther, T., Hileman, W., Plett, G.L., Trimboli, M.S., and Danzer, M.A.A. (2024). Demystifying the Distribution of Relaxation Times: A Simulation-Based Investigation into the Limits and Possibilities of Interpretation for Lithium-Ion Batteries. J. Electrochem. Soc.

13. Plank, C., Rüther, T., Jahn, L., Schamel, M., Schmidt, J.P., Ciucci, F., and Danzer, M.A. (2024). A review on the distribution of relaxation times analysis: A powerful tool for process identification of electrochemical systems. J. Power Sources *594*, 233845.

14. Caliandro, P., Nakajo, A., Diethelm, S., and van herle, J. (2019). Model-assisted identification of solid oxide cell elementary processes by electrochemical impedance spectroscopy measurements. J. Power Sources *436*, 226838.

15. Schomburg, F., Heidrich, B., Wennemar, S., Drees, R., Roth, T., Kurrat, M., Heimes, H., Jossen, A., Winter, M., Cheong, J.Y., and Röder, F. (2024). Lithium-ion battery cell formation: status and future directions towards a knowledge-based process design. Energy Environ. Sci. *17*, 2686–2733.

16. Katzer, F., Rüther, T., Plank, C., Roth, F., and Danzer, M.A. (2022). Analyses of polarisation effects and operando detection of lithium deposition in experimental half- and commercial full-cells. Electrochim. Acta *436*, 141401.

17. Iurilli, P., Brivio, C., and Wood, V. (2021). On the use of electrochemical impedance spectroscopy to characterize and model the aging phenomena of lithium-ion batteries: a critical review. J. Power Sources *505*, 229860.

18. Teliz, E., Zinola, C.F., and Díaz, V. (2022). Identification and quantification of ageing mechanisms in Li-ion batteries by Electrochemical impedance spectroscopy. Electrochim. Acta *426*, 140801.

19. Nejad, S., Gladwin, D.T., and Stone, D.A. (2016). A systematic review of lumped-parameter equivalent circuit models for real-time estimation of lithium-ion battery states. J. Power Sources *316*, 183–196.

20. Plett, G.L. (2015). Battery Management Systems (Artech House).

21. Wang, S., Zhang, J., Gharbi, O., Vivier, V., Gao, M., and Orazem, M.E. (2021). Electrochemical impedance spectroscopy. Nat. Rev. Methods Primers *1*, 41.

22. Khalik, Z., Donkers, M., Sturm, J., and Bergveld, H.J. (2021). Parameter estimation of the Doyle–Fuller–Newman model for Lithium-ion batteries by parameter normalization, grouping, and sensitivity analysis. J. Power Sources *499*, 229901.

23. Jokar, A., Rajabloo, B., Désilets, M., and Lacroix, M. (2016). Review of simplified Pseudo-two-Dimensional models of lithium-ion batteries. J. Power Sources *327*, 44–55.

24. Plett, G.L., and Trimboli, M.S. (2015-2024). Battery management systems. Physics-based Methods (Artech House).

25. Schmidt, J.P., Chrobak, T., Ender, M., Illig, J., Klotz, D., and Ivers-Tiffée, E. (2011). Studies on LiFePO4 as cathode material using impedance spectroscopy. J. Power Sources *196*, 5342–5348.

26. Hahn, M., Rosenbach, D., Krimalowski, A., Nazarenus, T., Moos, R., Thelakkat, M., and Danzer, M.A. (2020). Investigating solid polymer and ceramic electrolytes for lithium-ion batteries by means of an extended Distribution of Relaxation Times analysis. Electrochim. Acta *344*, 136060.

27. Danzer, M.A. (2019). Generalized Distribution of Relaxation Times Analysis for the Characterization of Impedance Spectra. Batteries *5*, 53.

28. Rüther, T., Gosea, I.V., Jahn, L., Antoulas, A.C., and Danzer, M.A. (2023). Introducing the Loewner Method as a Data-Driven and Regularization-Free Approach for the Distribution of Relaxation Times Analysis of Lithium-Ion Batteries. Batteries *9*, 132.

29. Dierickx, S., Weber, A., and Ivers-Tiffée, E. (2020). How the distribution of relaxation times enhances complex equivalent circuit models for fuel cells. Electrochim. Acta *355*, 136764.

30. Hahn, M., Schindler, S., Triebs, L.-C., and Danzer, M.A. (2019). Optimized Process Parameters for a Reproducible Distribution of Relaxation Times Analysis of Electrochemical Systems. Batteries *5*, 43.

31. Iurilli, P., Brivio, C., and Wood, V. (2022). Detection of Lithium-Ion Cells' Degradation through Deconvolution of Electrochemical Impedance Spectroscopy with Distribution of Relaxation Time. Energ. Tech. *10*.

32. Wan, T.H., Saccoccio, M., Chen, C., and Ciucci, F. (2015). Influence of the Discretization Methods on the Distribution of Relaxation Times Deconvolution: Implementing Radial Basis Functions with DRTtools. Electrochim. Acta *184*, 483–499.

33. Paul, T., Chi, P.W., Wu, P.M., and Wu, M.K. (2021). Computation of distribution of relaxation times by Tikhonov regularization for Li ion batteries: usage of L-curve method. Sci. Rep. *11*, 12624.

34. Saccoccio, M., Wan, T.H., Chen, C., and Ciucci, F. (2014). Optimal Regularization in Distribution of Relaxation Times applied to Electrochemical Impedance Spectroscopy: Ridge and Lasso Regression Methods - A Theoretical and Experimental Study. Electrochim. Acta *147*, 470–482.

35. Mayo, A.J., and Antoulas, A.C. (2007). A framework for the solution of the generalized realization problem. Lin. Algebra Appl. *425*, 634–662.

36. Gosea, I.V., Poussot-Vassal, C., and Antoulas, A.C. (2022). Data-driven modeling and control of large-scale dynamical systems in the Loewner framework. In Numerical Control: Part A (Elsevier), pp. 499–530.

37. (2017). MODEL Reduction and Approximation. Theory and Algorithms (Society for Industrial and Applied Mathematics).

38. Sorrentino, A., Patel, B., Gosea, I.V., Antoulas, A.C., and Vidaković-Koch, T. (2023). Determination of the distribution of relaxation times through Loewner framework: A direct and versatile approach. J. Power Sources *585*, 233575.

39. Antoulas, A.C., Lefteriu, S., and Ionita, A.C. (2017). Chapter 8: A Tutorial Introduction to the Loewner Framework for Model Reduction. In Model Reduction and Approximation, P. Benner, M. Ohlberger, A. Cohen, and K. Willcox, eds. (Society for Industrial and Applied Mathematics), pp. 335–376.

40. Antoulas, A.C., Beattie, C.A., and Gugercin, S. (2020). Interpolatory Methods for Model Reduction.

41. Plank, C., Ruther, T., and Danzer, M.A. (9272022). Detection of Non-Linearity and Non-Stationarity in Impedance Spectra using an Extended Kramers-Kronig Test without Overfitting. In 2022 International Workshop on Impedance Spectroscopy (IWIS) (: IEEE), pp. 1–6.

42. Shannon, C.E. (2001). A Mathematical Theory of Communication. Bell System Technical Journal *5*, 3–55.

43. Jia, D., Wu, L., and Fan, H.082006. A Measure for Residual Correlation with Whiteness Test and Information Entropy. In 2006 International Conference on Machine Learning and Cybernetics (: IEEE), pp. 1630–1635.

44. Frey, T., and Bossert, M. (2009). Signal- und Systemtheorie. (Wiesbaden: Vieweg+Teubner).

45. Gregori, J., García-Jareño, J.J., Keddam, M., and Vicente, F. (2007). A kinetic interpretation of a negative time constant in impedance equivalent circuits for the dissolution/passive transition. Electrochim. Acta *52*, 7903–7909.

46. Danaee, I., Jafarian, M., Forouzandeh, F., Gobal, F., and Mahjani, M.G. (2008). Kinetic interpretation of a negative time constant impedance of glucose electrooxidation. J. Phys. Chem. B *112*, 15933–15940.

47. Cartwright, K.V., Joseph, E., and Kaminsky, E.J. (2010). Finding the Exact Maximum Impedance Resonant Frequency of a Practical Parallel Resonant Circuit without Calculus.

48. Schneider, J., Tichter, T., Khadke, P., Zeis, R., and Roth, C. (2020). Deconvolution of electrochemical impedance data for the monitoring of electrode degradation in VRFB. Electrochim. Acta *336*, 135510.

49. Pivac, I., Halvorsen, I.J., Bezmalinovic, D., Barbir, F., and Zenith, F. (2020). Low-frequency EIS Intercept as a Diagnostic Tool for PEM Fuel Cells Degradation. Zenodo database. https://doi.org/10.5281/zenodo.3631156.

50. Rüther, T., Schamel, M., Plank, C., Schomburg, F., Röder, F., and Danzer, M.A. (2023). Cell-to-Cell-Variations of a Panasonic NCR18650B. Zenodo database. https://doi.org/10.5281/zenodo.8369275.

51. Weiß, A., Schindler, S., Galbiati, S., Danzer, M.A., and Zeis, R. (2017). Distribution of Relaxation Times Analysis of High-Temperature PEM Fuel Cell Impedance Spectra. Electrochim. Acta *230*, 391–398.

52. Schönleber, M., Klotz, D., and Ivers-Tiffée, E. (2014). A Method for Improving the Robustness of linear Kramers-Kronig Validity Tests. Electrochim. Acta *131*, 20–27.

53. Schiller, C.A., Richter, F., Gülzow, E., and Wagner, N. (2001). Validation and evaluation of electrochemical impedance spectra of systems with states that change with time. Phys. Chem. Chem. Phys. *3*, 374–378.

54. Danzer, M.A., Plank, C., and Rüther, T. (2024). Impedance Data for Various Electrochemical and Electrical Systems. Zenodo database. https://doi.org/10.5281/zenodo.10794584.

55. Plank, C., Rüther, T., and Danzer, M.A. (2024). Impedance Analysis with ELSA and DRT for Various Electrochemical and Electrical Systems. Zenodo database. https://doi.org/10.5281/zenodo.10794720.

56. Danzer, M.A., Plank, C., and Rüther, T. (2024). Electrochemical System Analysis - ELSA. Zenodo database. https://doi.org/10.5281/zenodo.11473099.